OXFORD

Human Molecular Genetics, 2015, Vol. 24, No. 10 2938–2951

doi: 10.1093/hmg/ddv056
Advance Access Publication Date: 12 February 2015
Original Article

ORIGINAL ARTICLE

Parkin-mediated mitophagy in mutant hAPP neurons and Alzheimer's disease patient brains

Xuan Ye, Xiaqin Sun, Valentin Starovoytov and Qian Cai*

Department of Cell Biology and Neuroscience, Rutgers, The State University of New Jersey, Piscataway, NJ 08854, USA

*To whom correspondence should be addressed. Tel: +1 8484451633; Fax: +1 7324451794; Email: cai@biology.rutgers.edu

Abstract

Accumulation of dysfunctional mitochondria is one of the hallmarks in Alzheimer's disease (AD). Mitophagy, a selective autophagy for eliminating damaged mitochondria, constitutes a key cellular pathway in mitochondrial quality control. Recent studies established that acute depolarization of mitochondrial membrane potential ($\Delta\psi_m$) using $\Delta\psi_m$ dissipation reagents *in vitro* induces Parkin-mediated mitophagy in many non-neuronal cell types or neuronal cell lines. However, neuronal pathways inducing mitophagy, particularly under pathophysiological relevant context in AD mouse models and patient brains, are largely unknown. Here, we reveal, for the first time, that Parkin-mediated mitophagy is robustly induced in mutant hAPP neurons and AD patient brains. In the absence of $\Delta\psi_m$ dissipation reagents, hAPP neurons exhibit increased recruitment of cytosolic Parkin to depolarized mitochondria. Under AD-linked pathophysiological conditions, Parkin translocation predominantly occurs in the somatodendritic regions; such distribution is associated with reduced anterograde and increased retrograde transport of axonal mitochondria. Enhanced mitophagy was further confirmed in AD patient brains, accompanied with depletion of cytosolic Parkin over disease progression. Thus, aberrant accumulation of dysfunctional mitochondria in AD-affected neurons is likely attributable to inadequate mitophagy capacity in eliminating increased numbers of damaged mitochondria. Altogether, our study provides the first line of evidence that AD-linked chronic mitochondrial stress under *in vitro* and *in vivo* pathophysiological conditions effectively triggers Parkin-dependent mitophagy, thus establishing a foundation for further investigations into cellular pathways in regulating mitophagy to ameliorate mitochondrial pathology in AD.

Introduction

Mitochondrial dysfunction is a prominent feature of both familial and sporadic Alzheimer's disease (AD) and plays an important role in AD pathophysiology (1,2). Brain imaging studies of AD patients suggest early metabolic changes prior to the onset of histopathological or clinical features, supporting the hypothesis that mitochondrial deficit is a key hallmark of AD (3). In addition to reduced cerebral metabolism in affected brain regions (4,5), altered mitochondrial structures have also been observed (6–8). Dysfunctional mitochondria not only produce energy and buffer Ca^{2+} less efficiently, but also release harmful reactive oxygen species (ROS) (9). These damaged mitochondria are progressively accumulated in axons and at synapses over the lifetime of AD-linked neurons, which is thought to contribute to the pathogenesis of neurodegeneration (10,11). These observations raise a fundamental question: are cellular mechanisms maintaining mitochondrial quality compromised in AD brains, thus augmenting mitochondria pathology?

Mitophagy, a cargo-selective autophagy for the removal of damaged mitochondria, constitutes a key cellular pathway in mitochondrial quality control. Recent studies have indicated that depolarized mitochondria recruit Parkin to initiate mitophagy for subsequent degradation within the autophagy–lysosomal pathway (12–16). However, these studies were mainly established on *in vitro* cell models by acute depolarization of mitochondrial membrane potential ($\Delta\psi_m$) using $\Delta\psi_m$ dissipation reagents or by light irradiation of mitochondrial ROS production. The critical understanding of whether and how AD-linked pathological

Received: October 4, 2014. **Revised and Accepted:** February 9, 2015

processes induce or affect Parkin-dependent mitophagy remains very limited, particularly in pathophysiology relevant context in the brains of AD-linked mouse models and human patients.

Accumulation of amyloid-β (Aβ) deposits as senile plaques is a pathological hallmark feature of AD. A growing body of evidence suggests that elevated Aβ levels contribute to mitochondrial abnormalities. Neurons derived from amyloid precursor protein (APP) transgenic (Tg) mouse models display altered mitochondrial dynamics, impaired trafficking and reduced biogenesis (17,18). Aβ has been found within mitochondrial membranes and interact with mitochondrial proteins, through which Aβ may affect mitochondrial dynamics, alter mitochondrial motility (17,19–22), disrupt electron transfer chain, increase ROS production (23–25) and impair mitochondrial function (19,26–28). Despite the well-documented Aβ-mediated mitochondrial dysfunction, it is not known whether mitophagy is efficiently induced under these pathophysiological conditions. In current study, we addressed this fundamental issue by live imaging of mutant hAPP Tg neurons and by examining AD patient brains using transmission electron microscopy (TEM) combined with mitochondrial purification. Our study reveals for the first time that Parkin-dependent mitophagy is robustly induced in mutant hAPP Tg neurons and AD patient brains, which is associated with an increased mitophagic flux. Mutant hAPP neurons exhibited enhanced recruitment of cytosolic Parkin to depolarized mitochondria. Parkin translocation predominantly occurs in the somatodendritic regions; such compartmental distribution is coupled with reduced anterograde transport of mitochondria in axons. Strikingly, enhanced mitophagy in AD patient brains was accompanied with depletion of cytosolic Parkin over disease progression. Therefore, the aberrant accumulation of defective mitochondria is likely attributed to inadequate mitophagy capacity in removing increased numbers of damaged mitochondria. Our results illustrate the intriguing AD-linked mitophagy profile and provide the first *in vivo* indication that Parkin is progressively depleted during the course of AD development, thus establishing a foundation for future investigations into up-regulation of mitophagy to maintain mitochondrial integrity in AD brains.

Results

AD-linked mitochondrial stress induces mitophagy in mutant hAPP Tg neurons

To examine whether mitochondria in mutant hAPP Tg neurons are in dysfunctional status, we first measured mitochondrial membrane potential ($\Delta\psi_m$) in cultured cortical neurons derived from WT and hAPP transgenic (Tg) mice harboring the human AD Swedish and Indiana mutations (J20) (29). Tetramethylrhodamine ethyl ester (TMRE), an $\Delta\psi_m$-dependent dye, was loaded into live neurons expressing mitochondrial marker CFP-Mito at 14–15 days *in vitro* (DIV). Healthy mitochondria accumulate TMRE, thus displaying high TMRE intensity (30), while dysfunctional mitochondria with depolarized $\Delta\psi_m$ show reduced TMRE fluorescent intensity although they retain CFP-Mito signals. In WT neurons, the majority of CFP-Mito-labeled mitochondria were co-labeled by TMRE, reflecting their electrochemically active status (Fig. 1A). In contrast, somatic mitochondria in mutant hAPP Tg neurons displayed reduced TMRE staining, suggesting depolarized $\Delta\psi_m$ (Fig. 1A). We quantified TMRE mean intensity in soma and normalized to that in WT neurons (Fig. 1B). Compared with WT neurons, mutant hAPP Tg neurons exhibited a substantial reduction in TMRE mean intensity to 66.93% ± 2.9% ($P < 0.001$), suggesting an accumulation of depolarized mitochondria. Our data provide the first live-cell evidence that mitochondria in AD neurons are under depolarized status, thus establishing an experimental foundation for our investigations into Parkin-mediated mitophagy in AD neurons under physiological and pathological conditions without incubation with any $\Delta\psi_m$ dissipating reagent with cell toxicity.

To examine whether autophagy is induced under chronic pathological conditions in AD-linked mouse brains, we performed sequential immunoblots of brain cortex homogenates from WT and hAPP Tg mice harboring the human AD Swedish and Indiana mutations (CaMKIIα-tTA X tet-APPswe/ind) (31). Compared with WT, increased autophagic marker LC3-II (2.35 ± 0.15; $P < 0.001$) and reduced Parkin intensity (0.547 ± 0.03; $P < 0.01$) were consistently detected in mutant hAPP Tg mouse brains while the markers for mitochondria (TOM20) (1.058 ± 0.18; $P = 0.777$) and Golgi (p115) (0.98 ± 0.04; $P = 0.66$) exhibited no detectable change (Fig. 1C and D). While elevated autophagic marker suggests increased autophagic flux, we also showed that depolarized mitochondria were accumulated in mutant hAPP Tg neurons (Fig. 1A and B). Thus, these results raise a possibility that mitophagy might be altered in AD neurons.

To address whether Parkin-mediated mitophagy is induced in mutant hAPP Tg mouse brains, we purified mitochondria-enriched fractions (Mito) from WT and mutant hAPP Tg mouse cortices using Percoll gradient centrifugation as previously described (32,33). Equal amounts of Mito and post-nuclear supernatants (PNS) were loaded for sequential immunoblotting. Strikingly, Parkin was remarkably increased in Mito fractions from mutant hAPP Tg mice (9.396 ± 1.23; $P < 0.01$), along with robustly increased autophagic markers LC3-II and p62 (45.48 ± 5.41, $P = 0.001$; 6.69 ± 1.16, $P < 0.01$, respectively) relative to WT mice (Fig. 1E and F). Moreover, elevated levels of APP and Aβ were associated with mitochondrial fractions in mutant hAPP mice. Consistently, Mito fraction purified from cultured neurons derived from mutant hAPP mouse brains also showed increased Parkin and LC3-II (Supplementary Material, Fig. S1).

Previous studies showed the accumulation of Aβ within mitochondria in AD brains (19,21,25,26), raising a question as to whether Aβ associates with Parkin-tagged depolarized mitochondria. To address this question, we immunoisolated Parkin-associated mitochondria from Mito fractions of WT and mutant hAPP Tg mouse brains using Dyna magnetic beads coated with an anti-Parkin antibody. APP and Aβ were readily detected in the purified Parkin-targeted mitochondria labeled by mitochondrial matrix protein HSP60 (Fig. 1G), which is resistant to Parkin-mediated proteasome-dependent degradation (34,35). To our knowledge, this is the first documented evidence that Aβ is associated with Parkin-targeted mitochondria in AD mouse brains.

Increased Parkin translocation to depolarized mitochondria in AD neurons

Increased oligomeric Aβ accumulation within mitochondria has been reported in cultured primary neurons from mutant hAPP Tg mice (17). We next asked whether mutant hAPP Tg neurons display progressively increased Parkin translocation to dysfunctional mitochondria over time in culture. Cortical neurons were co-transfected with YFP-Parkin and DsRed-Mito and imaged at various time points as indicated. While Parkin was diffuse in almost all WT neurons between DIV15 and DIV21, the percentage of total neurons displaying Parkin translocation to fragmented mitochondria was progressively increased in mutant hAPP Tg neurons after 2 weeks in culture (DIV 15: hAPP, 13.26 ± 2.37%;

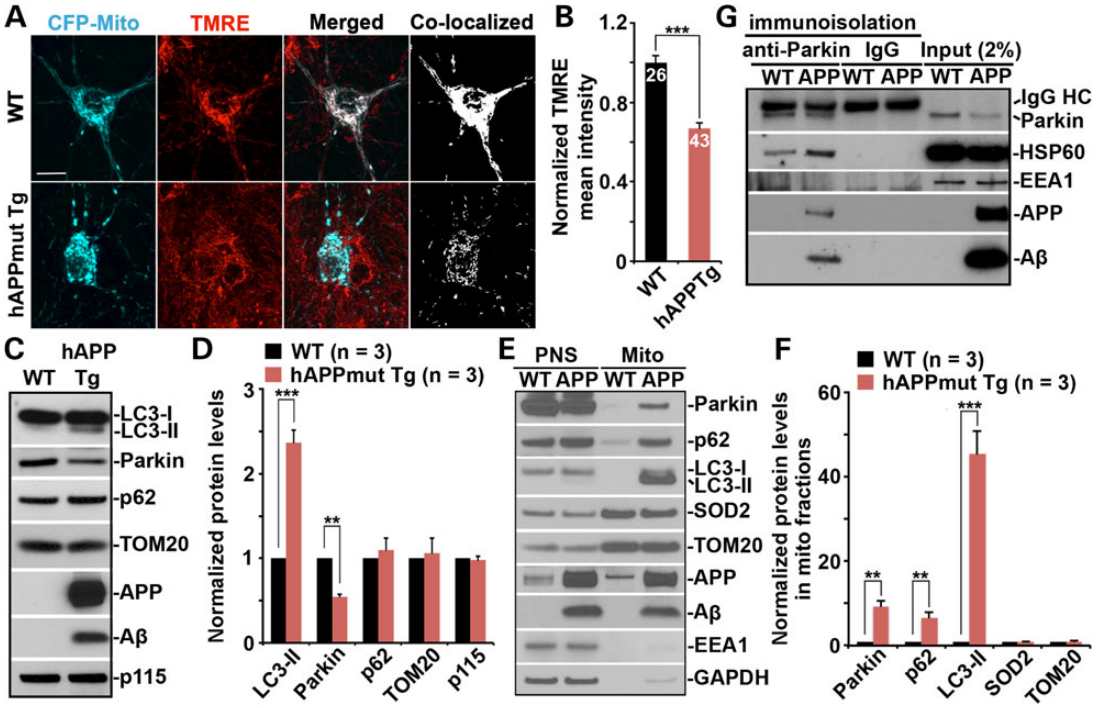

Figure 1. AD-linked mitochondrial stress induces mitophagy in mutant hAPP Tg neurons. (**A** and **B**) Representative images (A) and quantitative analysis (B) showing accumulation of depolarized mitochondria in mutant hAPP Tg neurons. Cortical neurons cultured from WT or mutant hAPP Tg mice were transfected with mitochondrial marker CFP-Mito, followed by loading with mitochondrial membrane potential ($\Delta\psi_m$)-dependent dye TMRE for 30 min prior to imaging. TMRE mean intensity was normalized to WT neurons. Note that hAPP mutant neurons displayed reduced TMRE mean intensity in the soma relative to that of WT neurons. Scale bars: 10 μm. Data were quantified from a total number of neurons as indicated in the bars (B) from > 3 independent experiments. (**C** and **D**) Representative blots (C) and quantitative analysis (D) showing altered mitophagy/autophagy markers in the brains of mutant hAPP Tg mice. A total of 20 μg of brain homogenates from WT and mutant hAPP Tg mice were sequentially detected on the same membrane. Relative protein levels were normalized by Golgi marker p115 and compared with that of WT littermates. (**E** and **F**) Increased mitochondrial association of Parkin, p62/SQSTM1 and LC3-II in the brains of mutant hAPP Tg mice. Following Percoll-gradient membrane fractionation, equal amount (5 μg) of mitochondria-enriched membrane fraction (Mito) and post-nuclear supernatant (PNS) from WT and mutant hAPP Tg mice were sequentially immunoblotted with antibodies against Parkin, autophagy markers p62 and LC3, mitochondrial markers SOD2 and TOM20, early endosome marker EEA1 and cytosolic protein GAPDH, along with APP and Aβ (6E10). The purity of Mito fractions was confirmed by the relative enrichment of mitochondrial markers SOD2 and TOM20 compared with PNS fractions, and by the absence of EEA1 and GAPDH. Relative protein levels in mitochondria-enriched membrane fraction of AD mice were compared with those in WT littermates. (**G**) Immunoisolation assay showing association of APP and Aβ with Parkin in mutant hAPP Tg mouse brains. Parkin-associated membranous organelles were immunoisolated from light membrane fractions with anti-Parkin-coated Dyna magnetic beads, followed by sequential immunoblotting on the same membranes after stripping between each antibody application. Data in C, D, E, F and G were analyzed from three pairs of mice for each genotype and expressed as mean ± SEM with Student's *t*-test: ***$P \leq 0.001$; **$P < 0.01$; *$P < 0.05$.

DIV 17: hAPP, 23.29 ± 4.17%; DIV19: hAPP, 34.1 ± 2.75%; DIV21: hAPP, 42.58 ± 0.97%) (Fig. 2A and B). The pattern of Parkin translocation in mutant hAPP Tg neurons is similar to that of WT neurons treated for 24 h with 10 μM carbonyl cyanide m-chlorophenyl hydrazone (CCCP), an $\Delta\psi_m$ dissipating reagent (Fig. 2A). Consistently, we observed increased percentage of WT neurons displaying Parkin translocation to fragmented mitochondria following overexpressing mutant hAPPswe (19.74 ± 1.68%, $P < 0.001$), but not WT hAPP (3.21 ± 0.32%, $P > 0.05$), relative to neurons expressing vector control (3.66 ± 0.37%) (Supplementary Material, Fig. S2A and B). In addition, we provided further evidence showing increased percentage of WT neurons with LC3-labeled mitophagosomes when overexpressing mutant hAPPswe (27.63 ± 1.70%, $P < 0.01$), compared with that of control neurons (8.35 ± 1.45%) (Supplementary Material, Fig. S2C and D), suggesting that mitophagy is induced in AD neurons.

We previously demonstrated that $\Delta\psi_m$ depolarization induces Parkin translocation to mitochondria in mature cortical neurons (30). To examine whether Parkin-targeted mitochondria display dissipated $\Delta\psi_m$, we loaded TMRE in live WT and mutant hAPP Tg neurons expressing YFP-Parkin and CFP-Mito. In WT or mutant hAPP Tg neurons showing diffused cytosol Parkin, the majority of CFP-Mito-labeled mitochondria were stained by TMRE, reflecting their electrochemically active status (Fig. 2C). In contrast, Parkin-targeted mitochondria in mutant hAPP Tg neurons exhibited reduced TMRE staining, suggesting $\Delta\psi_m$ depolarization (Fig. 2C). We quantified TMRE mean intensity in soma and normalized to that in WT neurons (Fig. 2D). While mutant hAPP neurons lacking Parkin translocation showed the similar TMRE mean intensity (91.31 ± 3.72%; $P = 0.223$) to WT controls, mutant hAPP neurons with Parkin translocation exhibited a significant reduction in TMRE mean intensity (42.33 ± 3.0%; $P < 0.001$), suggesting that Parkin was selectively recruited to depolarized mitochondria in mutant hAPP neurons. To further characterize Parkin-mediated mitophagy in AD neurons, we provided an evidence showing co-localization of Parkin-targeted mitochondria with endogenous p62/SQSTM1 in mutant hAPP Tg neurons (Fig. 2E). While this study suggests that Parkin-mediated mitophagy is predominantly induced in AD neurons, other Parkin-independent pathways may also be involved in AD-related mitochondrial quality control (36).

Extracellular Aβ can be internalized and taken up by mitochondria (37,38), thus Aβ plaques likely serve as focal sources of mitochondrial toxicity (39). To examine whether extracellular

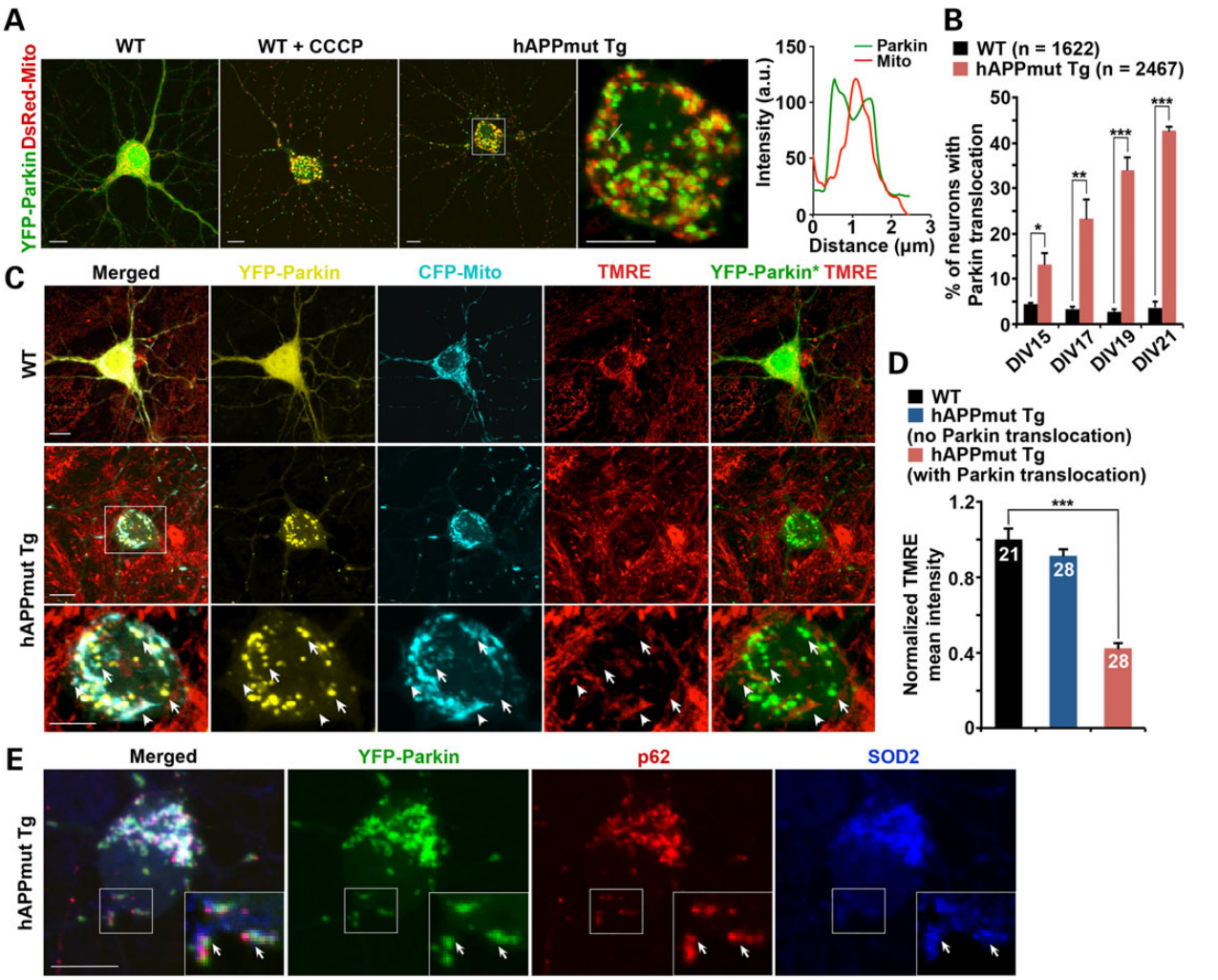

Figure 2. Increased Parkin translocation to depolarized mitochondria in mutant hAPP Tg neurons. (**A** and **B**) Representative images (A) and quantitative analysis (B) showing increased percentage of total mutant hAPP Tg neurons with Parkin translocation to fragmented mitochondria over time in culture. Cortical neurons were co-transfected with YFP-Parkin and DsRed-Mito, followed by imaging at DIV15, 17, 19 and 21, respectively. Graph to the right is a line scan of relative DsRed-Mito and YFP-Parkin fluorescence intensities from an enlarged image in the somatic area of the mutant hAPP Tg neuron (left panel). As $\Delta\psi_m$ dissipation control, WT neurons were treated with 10 μM CCCP for 24 h. Note that the percentage of total mutant hAPP neurons displaying Parkin localization to mitochondria was progressively increased after 2 weeks in culture in the absence of CCCP. (**C** and **D**) Representative images (C) and quantitative analysis (D) showing translocation of YFP-Parkin to depolarized mitochondria in mutant hAPP neurons. Cortical neurons from WT or mutant hAPP Tg mice were co-transfected with YFP-Parkin and CFP-Mito, followed by incubating with TMRE for 30 min prior to imaging. Note that mutant hAPP Tg neurons with no Parkin translocation displayed normal TMRE intensity, whereas neurons with Parkin recruitment showed reduced TMRE mean intensity in the soma relative to that of control neurons. Arrows indicate Parkin-targeted depolarized mitochondria labeled by CFP-Mito but unlabeled by TMRE; arrowheads represent relatively polarized 'healthy' mitochondria marked by both CFP-Mito and TMRE, but not labeled by Parkin. YFP-Parkin*: color converted from yellow to green for better contrast. TMRE mean Intensity from whole cells in the soma of mutant hAPP neurons was normalized to that in control neurons. (**E**) Representative images showing that mitochondria tagged by Parkin were co-localized with p62 in mutant hAPP Tg neurons. hAPP neurons were transfected with YFP-Parkin (green), followed by immunostaining for autophagy marker p62/SQSTM1 (red) and mitochondrial marker SOD2 (blue). Insets show an enlarged view of the boxed areas. Arrows mark Parkin punca labeled by p62 and SOD2. Scale bars: 10 μm. Data were quantified from a total number of neurons (*n*) as indicated in parentheses (B) or on the top of bars (D) from >3 independent experiments. Error bars: SEM. Student's *t*-test: $^{***}P < 0.001$; $^{**}P < 0.01$; $^{*}P < 0.05$.

application of oligomeric Aβ sufficiently induces Parkin-dependent mitophagy, we incubated non-Tg neurons with a relatively low concentration (500 nM) of oligomeric Aβ1–42. Increasing percentage of neurons displayed Parkin recruitment to mitochondria following 72–96 h incubation with Aβ1–42 oligomers (18.29 ± 2.48%; $P < 0.01$) relative to vehicle controls (4.50 ± 1.31%) (Supplementary Material, Fig. S2E). Such Aβ-induced Parkin translocation is selective for depolarized mitochondria with reduced TMRE mean intensity (54.92 ± 2.29%; $P < 0.001$) (Supplementary Material, Fig. S2F and G). In addition, we demonstrated that oligomeric Aβ treatment increased the percentage of non-Tg neurons displaying LC3-labeled mitophagosomes (4.18 ± 1.14% in vehicle control; 22.40 ± 1.41% in Aβ-treated, $P < 0.001$) and the average number of mitophagosomes per neuron (1.23 ± 0.12 in vehicle control; 4.0 ± 0.25 in Aβ-treated; $P < 0.001$) (Supplementary Material, Fig. S2H–K). Moreover, we showed that mitochondria tagged by Parkin were largely co-localized with endogenous p62 in neurons treated with Aβ1–42 oligomers (Supplementary Material, Fig. S2L). Our results suggest that AD neurons display increased Parkin recruitment to depolarized mitochondria, thus providing the first indication that AD-linked mitochondrial stress is sufficient to induce Parkin-mediated mitophagy.

Compartmental restriction of Parkin translocation and altered mitochondrial transport in mutant hAPP Tg neurons

We next examined the distribution pattern of Parkin-targeted mitochondria in mutant hAPP Tg cortical neurons. In the absence of any $\Delta\psi_m$ dissipating reagent, AD neurons display Parkin translocation to fragmented mitochondria predominantly accumulated in the somatodendritic regions but are hardly detectable in distal axons (Supplementary Material, Fig. S3). This unique compartmental distribution pattern was also consistently observed in our previous study in mature cortical neurons treated with $\Delta\psi_m$ dissipating reagent CCCP, Antimycin A or oligomycin (30). These results suggest two possibilities: AD-linked pathological stress depolarizes mitochondria selectively located within the soma or transported to the somatodendritic regions. Recent studies suggest the latter is more likely as Parkin translocation mediates degradation of mitochondria-outer-membrane proteins including KIF5 motor adaptor Miro (34,40–43).

To address whether altered mitochondrial transport following AD-linked pathological stress contributes to the observed compartmental distribution of Parkin-targeted mitochondria, we examined mitochondrial motility in mutant hAPP Tg neurons by focusing on axons given their uniform microtubule organization and polarity. Axonal processes were selected as we previously reported (30,44,45). Kymographs were used to quantify relative motility. In WT axons, ~39.62% of mitochondria are motile, where 22.18 ± 1.22% undergo anterograde transport and 17.44 ± 1.19% move in retrograde direction. In contrast, in mutant hAPP Tg neurons with somatic Parkin translocation, anterograde transport was reduced to 7.21 ± 1.22% ($P < 0.001$), whereas retrograde transport was relatively increased (23.26 ± 1.95%, $P < 0.05$) (Fig. 3A and B). As a control, mitochondrial motility in AD neurons displaying no Parkin translocation was similar to those in WT neurons (Fig. 3A and B). These results suggest that Parkin localization to mitochondria arrests anterograde transport of axonal mitochondria in mutant hAPP neurons, thus restricting Parkin-mediated mitophagy in somatodendritic regions, where mature lysosomes are mainly localized (44,46).

Aberrant accumulation of mitophagosomes in mutant hAPP Tg neurons and mouse brains

To determine whether Parkin-tagged mitochondria upon mitophagy induction in mutant hAPP Tg neurons are delivered to the autophagy pathway, we labeled autophagic vacuoles with GFP-LC3 as described in our previous studies (30,44). In WT neurons, GFP-LC3 was cytosolic (Fig. 4A). However, in AD neurons, GFP-LC3 was recruited to fragmented mitochondria in the somatodendritic regions, consistent with the unique distribution pattern of Parkin-targeted mitochondria (Supplementary Material, Fig. S3). The averaged number of LC3-labeled autophagosomes engulfing mitochondria (mitophagosomes) was significantly increased in mutant hAPP Tg neurons (5.47 ± 0.69; $P < 0.001$) relative to WT controls (1.15 ± 0.36) (Fig. 4B).

To further assess increased formation of mitophagosomes in hAPP neurons, we alternatively examined a second autophagic marker p62/SQSTM. Increased p62 ring-like structures were associated with mitochondrial matrix protein HSP60 (Fig. 4C) and mitochondrial inter-membrane protein cytochrome c (Supplementary Material, Fig. S4A) in the soma of AD neurons, reflecting enhanced formation of mitophagosomes. In contrast, p62 is predominantly diffuse in the cytosol of WT neurons (Fig. 4C). Compared with WT neurons, mutant hAPP neurons showed robust increases in both the percentage of neurons containing mitophagosomes (9.5 ± 1.48% in WT; 50.19 ± 6.0% in mutant hAPP Tg; $P < 0.001$) and the average number of mitophagosomes per neuron (1.39 ± 0.107 in WT; 5.8 ± 0.429 in mutant hAPP Tg; $P < 0.001$) (Fig. 4D and E). Moreover, accumulation of p62 structures in the somatodendritic regions of mutant hAPP neurons was further confirmed with an antibody against MAP2 (Supplementary Material, Fig. S4A). Thus our results consistently demonstrate enhanced flux of depolarized mitochondria into the autophagy degradation pathway in AD neurons.

We next examined the capability of mitophagy in WT and hAPP neurons in response to acute $\Delta\psi_m$ dissipation by further treating neurons with 10 μM CCCP or DMSO control at DIV13–14 for 24 h, followed by isolating mitochondria-enriched membrane fraction. Relative to DMSO controls, CCCP-treated hAPP neurons exhibited an increased retention of autophagic markers p62 ($P < 0.05$) and LC3-II ($P < 0.05$) in mitochondrial fractions, which is similar to those in WT controls (Fig. 4F and G). These results indicate that acute mitochondrial depolarization can further augment mitophagy by recruiting more damaged mitochondria to the autophagy pathway in mutant hAPP neurons. Thus, elevated levels of autophagic markers p62 and LC3-II in mitochondria-enriched fractions could be attributed to increased autophagic flux of mitochondria in more AD neurons. However, these autophagic intermediates may also be retained due to impaired degradation capacity in lysosomes of AD neurons.

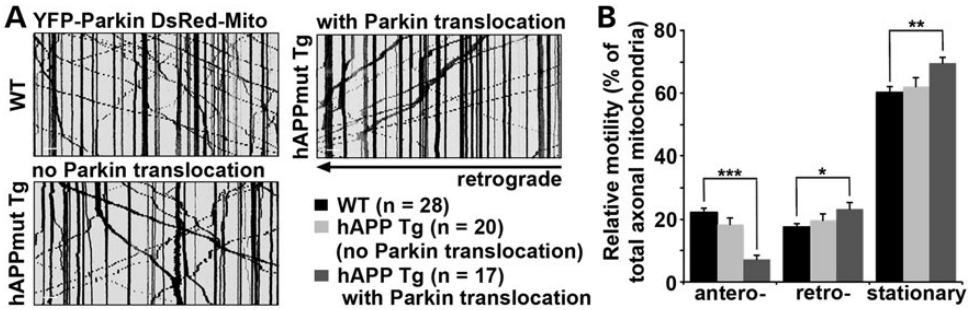

Figure 3. Altered mitochondrial transport in mutant hAPP Tg neurons with Parkin Translocation. (**A** and **B**) Representative kymographs (A) and quantitative analysis (B) showing altered motility of axonal mitochondria in mutant hAPP neurons during a ~9-min time-lapse imaging period. Vertical lines represent stationary organelles, oblique lines or curves to the right represent anterograde transport, and lines to the left indicate retrograde movement. Note that hAPP neurons with no Parkin translocation displayed unaltered motility, whereas neurons with Parkin translocation showed a reduced anterograde transport of axonal mitochondria. Data were quantified from a total number of neurons (*n*) as indicated in parentheses from >3 independent experiments. Scale bars: 10 μm. Error bars: SEM. Student's *t*-test: ***$P < 0.001$; **$P < 0.01$; *$P < 0.05$.

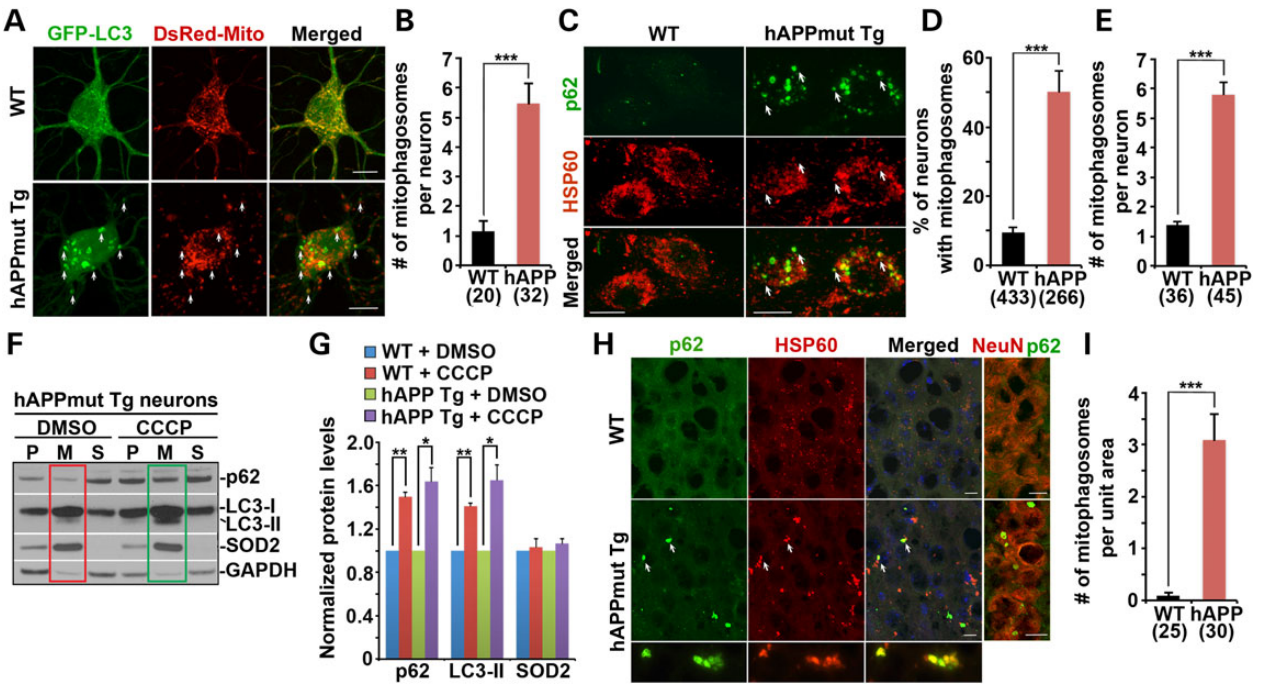

Figure 4. Aberrant accumulation of mitophagosomes in mutant hAPP Tg neurons and mouse brains. (**A** and **B**) Representative images (A) and quantitative analysis (B) showing enhanced LC3 recruitment to fragmented mitochondria in the soma of mutant hAPP neurons. Arrows indicate mitochondria engulfed in LC3-labeled autophagosomes. Mitochondria labeled with the autophagic marker LC3 are referred as mitophagosomes. Data were collected from >3 independent experiments. (**C–E**) Autophagic marker p62/SQSTM1 were recruited to mitochondria labeled by HSP60 (arrows) in the soma of hAPP neurons at DIV18–20 (C). Co-localization was analyzed as the percentage of neurons showing mitophagosomes (D) and the averaged number of mitophagosomes per neuron (E). Data were collected from three experiments. (**F** and **G**) $\Delta\psi_m$ dissipation with CCCP further augments mitophagy in mutant hAPP Tg neurons. WT or AD neurons at DIV13–14 were incubated with DMSO or 10 μM CCCP for 24 h and then subjected to fractionation into post-nuclear supernatant (P), mitochondrial-enriched membrane fraction (M) and cytosolic supernatant (S). An equal amount of protein (10 μg) was sequentially immunoblotted with antibodies against the autophagy markers p62/SQSTM1 and LC3, mitochondrial marker SOD2 and cytosolic protein GAPDH on the same membranes after stripping between each antibody application. Note that endogenous p62/SQSTM1 and LC3-II displayed an increased association with mitochondria following $\Delta\psi_m$ dissipation in hAPP neurons (green box) relative to DMSO control (red box). Data were quantified from three repeats. (**H** and **I**) Increased targeting of p62/SQSTM1 to clustered mitochondria (arrows) in the soma of the hippocampus of mutant hAPP Tg mice. Data were expressed as the average number of p62-labeled mitophagosomes per hippocampal slice section (320 μm × 320 μm). Scale bars: 10 μm. Data were quantified from a total number of neurons (B, D, E) or a total number of hippocampal sections (I) indicated in parentheses. Error bars: SEM. Student's *t*-test: $^{***}P < 0.001$; $^{**}P < 0.01$; $^{*}P < 0.05$.

To confirm the accumulation of mitophagosomes *in vivo*, we examined the hippocampus of the mutant hAPP Tg mouse brains. In WT mice, p62 appeared as a diffuse pattern in the cytosol of the soma. However, mutant hAPP Tg mouse brains exhibited clustered mitophagosomes co-labeled with p62 and HSP60. The average number of mitophagosomal-like structures per slice section was substantially increased relative to WT controls (WT: 0.096 ± 0.057; mutant hAPP Tg: 3.093 ± 0.495; $P < 0.001$) (Fig. 4H and I). A similar mitophagosomal clustering was consistently observed by immunostaining with an antibody against cytochrome *c* (Supplementary Material, Fig. S4B). These mitophagosomes were mainly located in the soma co-labeled by an anti-NeuN antibody (Fig. 4H). Thus, our findings from cultured mutant hAPP neurons and mouse brains support our notion that mitophagosomes are predominantly distributed in the somatodendritic regions, where mature lysosomes are mainly located (44,46). In addition, a significant number of mitophagosomes labeled by p62/SQSTM1 was co-localized with LAMP-1-marked lysosomes in the soma of hippocampal regions of AD mouse brains (Supplementary Material, Fig. S4C). Consistently, we also observed increased retention of fragmented mitochondria within clustered and enlarged LAMP-1-labeled degradative organelles in mutant hAPP Tg neurons (6.64 ± 0.51, $P < 0.001$) relative to non-Tg neurons (2.71 ± 0.32) (Supplementary Material, Fig. S4D and E). These results suggested both increased autophagic flux and defective clearance of autophagic substrates in AD neurons. Thus, Parkin localization to mitochondria could reflect accumulation of defective mitochondria in AD neurons rather than its direct involvement in AD pathology.

Enhanced Parkin-mediated mitophagy in AD patient brains

Mitochondrial dysfunction occurs in both familial and sporadic forms of AD (3). To determine Parkin-dependent mitophagy in AD patient brains, we isolated mitochondria-enriched fractions (Mito) from brains of AD patients and control subjects. The relative mitochondrial enrichment was confirmed by enhanced mitochondrial markers TOM20 and SOD2, and by the absence of early endosome marker EEA1 and cytosolic protein GAPDH. When equal amounts of Mito fractions and post-nuclear supernatants (PNS) were loaded, elevated levels of Parkin ($P = 0.0019$) along with robustly increased LC3-II levels ($P = 0.0012$) were detected in mitochondrial fractions from AD brains relative to those in control subjects (Fig. 5A and B). These results are consistent with those from mutant hAPP Tg mouse neurons (Fig. 1E and F), suggesting mitophagic augmentation in AD brains.

Using transmission electron microscopy (TEM), we next assessed autophagic accumulation and altered mitochondrial structures in hippocampus of AD patients and control subjects.

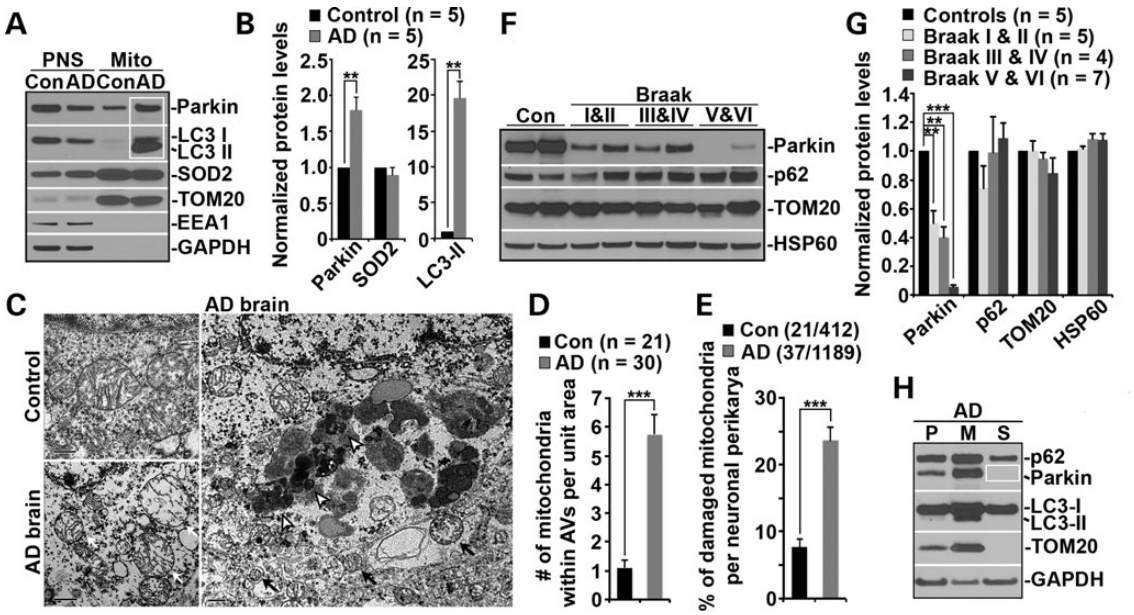

Figure 5. Parkin-mediated mitophagy in AD patient brains. (**A** and **B**) Increased levels of Parkin and LC3-II associated with purified mitochondria from AD patient brains. Following Percoll-gradient membrane fractionation, equal amount (5 μg) of mitochondria-enriched membrane fractions (Mito) and post-nuclear supernatant (PNS) fractions from brains of control and AD patients were sequentially immunoblotted with antibodies against Parkin and various markers including LC3 (autophagy), TOM20 and SOD2 (mitochondria), EEA1 (early endosome) and GAPDH (cytosol). Data were quantified from five independent repeats. (**C–E**) Representative TEM micrographs showing a striking accumulation of autophagic vacuoles (AVs) engulfing abnormal mitochondria in the hippocampus of AD patients (C). Clustered AV-like organelles and abnormal mitochondria with swollen shape and loss of cristae integrity were consistently observed in neuronal perikarya of AD patient brains. Quantitative analysis was expressed as the average number of mitochondria within AV-like organelles (D) and percentage of morphologically abnormal mitochondria (E) per neuronal perikarya in the cross section (10 μm × 10 μm). While black open arrows point to AVd-like organelles, black solid arrows mark AVi-like structures engulfing or containing damaged mitochondria. White arrows denote swollen mitochondria with perturbed or loss of inner structure in AD brain. Data were quantified from a total number of cells (*n*) (D) or a total number of cells and mitochondria (E) as indicated in parentheses from four different AD brains and two control brains. Scale bars: 500 nm. (**F** and **G**) Representative blots (F) and quantitative analysis (G) showing progressive Parkin reduction in AD patient brains. Twenty micrograms of brain homogenates from the cortices of age-matched controls and AD patients were sequentially detected on the same membrane. Relative protein levels were normalized to those of control subjects. Note that reduced Parkin levels were consistently observed in AD patient brains. Data were analyzed from the number of human brain samples as indicated in parentheses. (**H**) Representative blots showing depletion of cytosolic Parkin in AD patient brains. AD cortical tissues were subjected to fractionation into post-nuclear supernatant (P), mitochondrial-enriched membrane fraction (M) and cytosolic supernatant (S). An equal amount of protein (5 μg) of the three fractions was sequentially immunoblotted with antibodies against autophagy markers p62/SQSTM1, Parkin and LC3, mitochondrial marker TOM20 and cytosolic protein GAPDH on the same membranes after stripping between each antibody application. Error bars: SEM. Student's *t*-test: $^{***}P < 0.001$; $^{**}P < 0.01$; $^{*}P < 0.05$. APP, amyloid precursor protein; Aβ, amyloid-β; AD, Alzheimer's disease; WT, wild-type; Tg, transgenic; DIV, days *in vitro*; TMRE, tetramethylrhodamine ethyl ester; CCCP, carbonyl cyanide m-chlorophenyl hydrazone; Cyto c, cytochrome c; $\Delta\psi_m$, mitochondrial membrane potential; AV, autophagic vacuole; LAMP-1, lysosome-associated membrane protein-1; LC3, microtubule-associated protein light chain 3; Mito, mitochondria.

Mitochondria in AD brains exhibited abnormal morphology, characterized by swollen round shape and perturbed or loss of cristae organization. A striking accumulation of autophagic vacuoles (AVs)-like organelles was readily detected in AD hippocampus (Fig. 5C, black solid and open arrows), which is very rare in control brains. We also observed AVi-like structures engulfing or containing abnormal mitochondria (Fig. 5C, black solid arrows). The average number of mitochondria within AV-like organelles per unit area in neuronal perikarya is markedly increased in AD brains (Control: 1.10 ± 0.26; AD: 5.73 ± 0.72; $P < 0.001$) (Fig. 5D). This finding is consistent with our biochemical results showing increased levels of Parkin and LC3-II in mitochondria-enriched fractions (Fig. 5A and B), suggesting an elevated mitophagy induction in AD brains. However, damaged mitochondria with altered morphology per neuronal perikarya (white arrows) were significantly increased in AD brains (Control: 7.67 ± 1.26; AD: 23.65 ± 1.98; $P < 0.001$) (Fig. 5C and E), raising the possibility that mitophagy in AD brains is not induced to the full capacity for removing increased numbers of damage mitochondria.

To test this possibility, we compared relative Parkin levels in postmortem cortical tissues from Braak stages I and II (early), III and IV (definite) and V and VI (severe) AD patients and control subjects. Strikingly, we observed a progressive reduction in Parkin levels in the brains from a total of 16 AD patients (Braak I & II: 0.50 ± 0.09; $P < 0.01$; Braak III & IV: 0.40 ± 0.069; $P < 0.01$; Braak V & VI: 0.057 ± 0.014; $P < 0.001$) (Fig. 5F and G). Such a reduction was not observed in control subjects. Parkin levels were also decreased by 45.3 ± 0.03% in mutant hAPP Tg mouse brains (Fig. 1C and D). Progressive Parkin reduction in AD patient brains reflects an enhanced Parkin translocation to defective mitochondria and subsequent degradation upon mitophagy induction (40,42). Analysis of membrane fractionation further demonstrated depletion of cytosolic Parkin in AD patient brains (Fig. 5H). This is further supported by the fact that there is no significant change in mRNA levels of PARK2 in AD patient brains ($P > 0.05$) (Supplementary Material, Fig. S5A and B). In summary, our results illustrate the intriguing profile of AD-linked mitophagy and provide the first *in vivo* indication that progressive Parkin depletion at late AD stages is correlated with relative deficiency in mitophagy for removal of increased numbers of damaged mitochondria, thus establishing a foundation for future investigations into up-regulation of Parkin-mediated mitophagy in AD brains.

Discussion

Mitochondria support various neuronal functions and survival by generating ATP, buffering calcium and releasing signaling factors. Neurons face unique challenges in maintaining energy supply in distal processes and in maintaining functionality over the lifespan of an individual in the absence of self-renewal cell division. Growing evidence suggests that mitochondrial abnormalities occur at the early stage of the disease process in both genetic and non-genetic forms of AD (3). AD brains display aberrant accumulation of ultrastructurally altered mitochondria such as reduced size and broken internal membrane cristae (6,18). Investigation into neuronal regulation of mitochondrial quality control through mitophagy is fundamentally essential to advance our understanding of the pathophysiological processes in AD brains.

Recent studies in many non-neuronal cell types or neuronal cell lines established that efficient degradation of dysfunctional mitochondria through Parkin-dependent mitophagy is a key cellular pathway for maintaining mitochondrial integrity and function (16). Acute depolarization of mitochondrial $\Delta\psi_m$ *in vitro* with $\Delta\psi_m$ dissipation reagents induces Parkin-mediated mitophagy and subsequently eliminates depolarized mitochondria within the autophagy–lysosomal system. However, little is known about neuronal mitophagy under AD-linked pathological conditions. Our current study provides insights into Parkin-dependent mitophagy in AD-linked neurons and AD patient brains: (i) AD-linked mitochondrial stress is sufficient to induce Parkin-mediated mitophagy in mutant hAPP Tg neurons and mouse brains (Fig. 1 and Supplementary Material, Fig. S1); (ii) AD neurons exhibit increased Parkin recruitment selective to depolarized mitochondria in the absence of any $\Delta\psi_m$ dissipation reagent. Parkin-targeted mitochondria are largely co-localized with autophagy marker p62/SQSTM1 (Fig. 2 and Supplementary Material, Fig. S2); (iii) Parkin translocation is compartmentally restricted to the somatodendritic regions in AD neurons, coupled with reduced anterograde transport of axonal mitochondria in pathophysiological relevant context (Fig. 3 and Supplementary Material, Fig. S3); (iv) Mitophagosomes are aberrantly accumulated in mutant hAPP Tg neurons and mouse brains (Fig. 4 and Supplementary Material, Fig. S4); (v) Parkin-mediated mitophagy is confirmed in AD patient brains. More strikingly, AD patient brains display depletion of cytosolic Parkin over disease progression (Fig. 5). Thus, our study reveals, for the first time, that AD-linked mitochondrial stress signal sufficiently induces Parkin-dependent mitophagy in mutant hAPP neurons. Furthermore, we provided *in vivo* indication that the aberrant accumulation of dysfunctional mitochondria in AD brains can be attributed to inadequate mitophagy capacity for the removal of increased numbers of damaged mitochondria, thus setting the stage for future investigations into genetic and pharmacological dissection of factors that influence neuronal mitochondrial quality maintenance in AD brains.

Progressive accumulation of mitochondrial Aβ in postmortem AD patient brains, cellular and transgenic mouse models has been well documented, which is directly linked to mitochondrial toxicity (17,19,20,25,37,47). Our study demonstrates that AD-linked mitochondrial stress sufficiently induces mitophagy in mutant hAPP Tg neurons in the absence of any $\Delta\psi_m$ dissipation reagent (Figs 2 and 4). Total number of mutant hAPP neurons displaying Parkin translocation to mitochondria was increased over time in culture (Fig. 2), suggesting enhanced mitophagy. Reduction in $\Delta\psi_m$ and the emergence of dystrophic and fragmented mitochondria was shown to be limited to the vicinity of Aβ plaques in a live AD mouse model (39), suggesting a potential role of extracellular Aβ in mitochondrial alterations. Studies showed that extracellular Aβ was internalized and then imported into mitochondria in neuroblastoma cells and primary hippocampal neurons (37,38). Non-Tg neurons exhibited alterations in mitochondrial dynamics and motility upon incubation with extracellular Aβ (20,48,49), thus raising an important question as to whether extracellular Aβ-mediated mitochondrial stress serves as a signal triggering mitophagy. In current study, we addressed this issue by incubating WT neurons with a low concentration (500 nM) of Aβ. Strikingly, Aβ-treated WT neurons exhibited increased Parkin recruitment to depolarized mitochondria and mitophagosome formation (Supplementary Material, Fig. S2E–L), which is a phenomenon that is not readily detected in the absence of any $\Delta\psi_m$ dissipation reagent. To our knowledge, this is the first documented evidence revealing that both extracellular and intracellular Aβ-mediated mitochondrial stress sufficiently induces Parkin-dependent mitophagy.

Recent studies showed Parkin-mediated mitophagy of damaged mitochondria in distal axons following acute treatment of cultured neurons with a high concentration (40–80 μM) of Antimycin A, an inhibitor of respiratory complex III (43,50). In contrast, we took alternative procedure in our previous study: chronic treatment of mature cortical neurons with ten times lower concentrations of Antimycin A (1 μM), oligomycin (1 μM), or CCCP (10 μM). Under these mitochondrial stress conditions, the majority of neurons survive and mitochondria remain highly motile after 24 h treatment. We consistently demonstrated that Parkin-targeted damaged mitochondria are predominantly restricted in the soma accompanied with increased retrograde and reduced anterograde mitochondrial transport (30,51). In current study, we further confirmed this distribution pattern under AD-linked pathophysiological condition in the absence of any $\Delta\psi_m$ dissipation reagent. Parkin translocation to depolarized mitochondria is robustly induced predominantly in the soma of live AD neurons (Fig. 2, Supplementary Material, Fig. S2 and S3). We also provided *in vivo* evidence showing an increased mitophagic flux in the soma of hAPP neurons and mouse brains (Fig. 4 and Supplementary Material, Fig. S4). Our EM study further demonstrated the accumulation of defective mitochondria within autophagic vacuoles in neuronal perikarya of AD patient brains (Fig. 5C and D), which is consistent with previous observation showing an increased mitochondrial turnover by autophagy within the cell body in AD patient brains (7,8,52). Thus, our *in vitro* and *in vivo* findings from mutant hAPP Tg neurons and AD patient brains indicate that Parkin-dependent mitophagy occurs predominantly in the soma, where mature lysosomes are mainly located. Our findings are supported by a recent study showing predominant retrograde transport of autophagosomes including those engulfing damaged mitochondria from distal axons to the soma for more efficient degradation within acidic lysosomes enriched in the proximal regions of neurons (53).

Our study in mutant hAPP Tg neurons consistently shows reduced anterograde and enhanced retrograde transport of axonal mitochondria upon induction of Parkin translocation in the absence of any $\Delta\psi_m$ dissipation reagent (Fig. 3A and B). Our findings are consistent with recent studies showing Parkin-mediated degradation of anterograde transport motor adaptor Miro on the mitochondrial surface upon $\Delta\psi_m$ dissipation-induced mitophagy (34,40–43). Turnover of Miro on the mitochondrial surface may favor their retrograde transport to the soma. It is also possible that damaged mitochondria at distal processes can recruit Parkin for mitophagy once they are anchored by SNPH (30) or immobilized by degradation of motor adaptors (43). Given that mature

lysosomes are predominantly located in the soma, altered mitochondrial motility upon mitophagy induction may facilitate efficient elimination of mitochondria within the autophagy–lysosomal system. Studies showed that primary neurons from Tg2576 mice exhibited reduced anterograde transport of mitochondria along axons, which was rescued by a mitochondria-targeted antioxidant that decreased the percentage of defective mitochondria (17). Together with our results (Fig. 3), we proposed that upon Parkin translocation to depolarized mitochondria, enhanced degradation of Miro on mitochondrial surface contributes to reduced anterograde transport of axonal mitochondria in AD neurons. Application of mitochondria-targeted antioxidant may protect mitochondria from damage, thereby attenuating Parkin-mediated degradation of Miro. On the other hand, altered motility may be protective under chronic mitochondrial stress conditions in AD neurons; healthy mitochondria remain distally while damaged ones return to the soma for degradation. This spatial distribution allows neurons to efficiently remove dysfunctional mitochondria via the autophagy–lysosomal pathway in the soma.

Our study demonstrated that mutant hAPP Tg neurons and AD patient brains displayed mitophagy induction (Figs 1, 4 and 5). Autophagic vacuole-like organelles engulfing abnormal mitochondria were readily detected in neuronal perikarya (Fig. 5C and D). Enhanced Parkin-dependent mitophagy supports a notion that vulnerable AD neurons have increased mitophagic flux, attributable to increased mitochondrial damage. Although aberrant induction of autophagy has been indicated in AD brains (54,55), it is largely unknown what cellular basis contributes to altered autophagy in affected AD neurons. Our study provides a possible clue that enhanced induction of mitophagy–autophagy contributes to increased autophagic flux in AD. Our results consistently demonstrated undetectable change in mitochondrial markers in AD brains (Figs 1 and 5). Deficits in lysosomal degradation capacity have been implicated in AD, leading to accumulation of proteolytic substrates (46,56–58). A previous study also reported prominent autophagic accumulation of mitochondria in AD brains (8). We provided further evidence showing that p62-labeled mitophagosomes were largely co-localized with LAMP-1-marked lysosomes in the soma of hippocampal regions of AD mouse brains (Supplementary Material, Fig. S4C), suggesting defects in clearance of mitophagic intermediates. We also observed increased retention of fragmented mitochondria within clustered and enlarged LAMP-1-labeled degradative organelles in mutant hAPP Tg neurons (Supplementary Material, Fig. S4D and E). These results also suggest a deficit in lysosomal proteolysis, thus resulting in defects in removing accumulated mitophagosomes in AD brains. Parkin-mediated mitophagy induction associates with reduced levels of mitochondrial outer membrane proteins including TOM20 through proteasome-mediated protein degradation (34,35). Deficits in proteasome activity and inhibition of ubiquitin-dependent protein degradation have also been indicated in AD (59–61), which may contribute to unchanged levels of TOM20 in AD brains. Altogether, our findings support a notion that increased recruitment of Parkin and autophagic markers to depolarized mitochondria could be attributed to both increased autophagic flux and defective clearance of autophagic substrates due to increased mitochondrial stress or dysfunction in AD neurons.

In summary, our findings provide the cellular insights into the complex regulation of mitochondrial quality through Parkin-dependent mitophagy in response to AD-associated mitochondrial damage or stress in AD neurons. These results allow us to propose a model that enhancement of Parkin-mediated mitophagy facilitates elimination of dysfunctional mitochondria through the autophagy–lysosomal pathway. Further therapeutic approaches aimed at modulating mitophagy may help attenuate mitochondrial pathology associated with AD.

Materials and Methods

Mice

CaMKIIα-tTA and tet-APPswe/ind mice were obtained from H. Cai (National Institute on Aging, NIH, Bethesda, MD, USA). hAPP mice (C57BL/6J) from line J20 (29) were purchased from the Jackson Laboratory.

Human brain specimens

Fifteen postmortem brain specimens from AD patients and age-matched control subjects were obtained from the Harvard Tissue Resource Center, and the Human Brain and Spinal Fluid Resource Center at UCLA. Sixteen specimens were from patients diagnosed with AD according to Braak criteria (62), and five were from age-matched control subjects. On the basis of quantitative pathological features, including senile plaques, neurofibrillary tangles and neuronal density, the brain specimens were classified as specimens from Braak stage I and II (early AD), III and IV (definite AD), V and VI (severe AD) or control subjects. The specimens were from the frontal cortex and were both quick-frozen (BA9).

Materials

Sources of antibodies or reagents are as follow: polyclonal antibodies against LC3 and p62/SQSTM1 (MBL), HSP60 (Cell Signaling Technology), SOD2 (Sigma); TOM20, EEA1 and MAP2 (Santa Cruz); monoclonal antibodies against Parkin (Santa Cruz), GAPDH (Millipore/CHEMICON), p115, EEA1, MAP2 and cytochrome c (BD Biosciences), p62/SQSTM1 (Abnova), NeuN (Millipore), β Amyloid (6E10) and (4G8) (Covance); Alexa fluor 488-, 546- and 633-conjugated secondary antibodies (Invitrogen); TMRE (Invitrogen); CCCP (Calbiochem); Z-VAD-FMK and DMSO (Sigma-Aldrich).

Transfection and immunocytochemistry of cultured cortical neurons

Cortices were dissected from E18–19 mouse embryos as described (3,30,44). Cortical neurons were dissociated by papain (Worthington) and plated at a density of 100 000 cells per cm^2 on polyornithine- and fibronectin-coated coverslips. Neurons were grown overnight in plating medium (5% FBS, insulin, glutamate, G5 and 1 × B27) supplemented with 100× L-glutamine in Neurobasal medium (Invitrogen). Starting at DIV 2, cultures were maintained in conditioned medium with half-feed changes of neuronal feed (1 × B27 in Neurobasal medium) every 3 days. Primary hAPP Tg neurons were cultured from breeding mice of hemizygous mutant hAPPSwe/Ind Tg (J20 line) with WT animals (29). Genotyping assays were performed following culture plating to verify mouse genotypes. In our study, we examined both transgenic neurons and non-transgenic neurons derived from their littermates. WT and mutant hAPP Tg neurons were transfected with various constructs at DIV6–8 using Lipofectamine 2000 (Invitrogen) followed by 30 min pulse with 50 nm TMRE dye before imaging, or time-lapse imaging 7–13 days after transfection prior to quantitative analysis. For mitochondrial depolarization, WT cortical neurons were treated for 24 h with 50 μM Z-VAD-FMK and 10 μM CCCP prior to live imaging analysis as described previously (30).

For immunostaining, cultured neurons were fixed with 4% formaldehyde (Polyscience, Inc.) and 4% sucrose (Sigma) in 1× phosphate-buffered saline (PBS) at room temperature (RT) for 20 min, or 100% ice-cold methanol at −20°C for 10 min, washed three times with PBS for 5 min each, and then incubated in 0.4% saponin, 5% normal goat serum (NGS) and 2% bovine serum albumin (BSA) in PBS for 1 h. Fixed cultures were incubated with primary antibodies in PBS with 2% BSA and 0.4% saponin at 4°C overnight. Cells were washed four times with PBS at RT for 5 min each, incubated with secondary fluorescent antibodies at 1:400 dilution in PBS with 2% BSA and 0.4% saponin for 30 min, re-washed with PBS and then mounted with Fluor-Gel anti-fade mounting medium (EMS) for imaging.

Cell/Tissue fractionation and immunoblotting

Mitochondria-enriched membrane was prepared as previously described (30). Briefly, WT or mutant hAPP Tg cortical neurons were cultured in 100-mm plates at a density of 5×10^6 and treated with DMSO or 10 μM CCCP at DIV 13. After washing once with PBS, cells were harvested and suspended in ice-cold Isolation Buffer (IB) [10 mM Tris–HCl, 1 mM EGTA, 1 mM EDTA, 0.25 M sucrose and protease inhibitors (Roche), pH7.4]. Cells were then homogenized 20 times by passing through a 25-gauge needle using a 1-ml syringe on ice. For fractionation, human brain tissues (100 mg) were homogenized in ice-cold IB buffer. Following centrifugation of homogenates from cells or brains at 1000*g* for 10 min at 4°C, the supernatant was saved as post-nuclear supernatant (PNS). PNS was centrifuged at 15 000*g* for 10 min to separate the mitochondria-enriched fraction (Mito) from the cytosol-enriched fraction (Sup). The same amount of protein (5–10 μg) from each fraction was resolved by 4–12% Bis–Tris PAGE for sequential western blots on the same membranes after stripping between each application of antibody.

Tissue preparation and immunohistochemistry

Animals were anesthetized with 2.5% avertin (0.5 ml per mouse), and transcardially perfused with fixation buffer (4% paraformaldehyde in PBS, pH 7.4). Brains were dissected out and post fixed in fixation buffer overnight and then placed in 30% sucrose at 4°C. 10-μm-thick coronal sections were collected consecutively to the level of the hippocampus and used to study co-localization of various markers. After incubation with blocking buffer (2.5% goat serum, 0.15% Triton X-100, 1.5% BSA, 0.5% glycine in H_2O) at RT for 1 h, the sections were incubated with primary antibodies at 4°C overnight, followed by incubation with secondary fluorescence antibodies at 1:400 dilution at RT for 1 h. After fluorescence immuno-labeling, the sections were stained with DAPI and washed three times in PBS. The sections were then mounted with anti-fading medium (vector laboratories, H-5000) for imaging.

Image acquisition and quantification

Confocal images were obtained using an Olympus FV1000 oil immersion ×60 objective (1.3 numerical aperture) with a sequential-acquisition setting. For fluorescent quantification, images were acquired using the same settings below saturation at a resolution of 1024 × 1024 pixels (12 bit). Eight to ten sections were taken from the top-to-bottom of the specimen and brightest point projections were made. Morphometric measurements were performed using NIH ImageJ. Measured data were imported into Excel software for analysis. The thresholds in all images were set to similar levels. Fluorescence intensity of TMRE was expressed in arbitrary units of fluorescence per square area. The mean intensity of TMRE in the soma of mutant hAPP Tg cortical neurons was normalized as a percentile ratio relative to that in WT control cells. Data were obtained from at least three independent experiments and the number of cells or mitochondria used for quantification is indicated in the figures. All statistical analyses were performed using the Student's *t*-test and are presented as mean ± SEM.

Criteria for axon selection in cultured neurons

For analyzing mitochondrial motility in live neurons, we selected axons for time-lapse imaging and measuring mitochondrial motility because axons, but not dendrites, have a uniform microtubule organization and polarity. Axonal processes were selected as we previously reported (30,44,45). Briefly, axons in live images were distinguished from dendrites based on known morphological characteristics: greater length, thin and uniform diameter, and sparse branching (63). Only those that appeared to be single axons and separate from other processes in the field were chosen for recording axonal mitochondrial transport. Regions where crossing or fasciculation occurred were excluded from analysis.

For live cell time-lapse imaging, neurons were transferred to Tyrode's solution containing 10 mM HEPES, 10 mM glucose, 1.2 mM $CaCl_2$, 1.2 mM $MgCl_2$, 3 mM KCl and 145 mM NaCl, pH 7.4. Temperature was maintained at 37°C with an air stream incubator. Cells were visualized with a ×60 oil immersion lens (1.3 numerical aperture) on an Olympus FV1000 confocal microscope, using 458 excitation for CFP, 488 nm for GFP or YFP and 559 nm for TMRE or DsRed. Time-lapse sequences of 1024 × 1024 pixels (8 bit) were collected at 5-s intervals with 1% intensity of the laser to minimize laser-induced bleaching and cell damage while maximizing pinhole opening. Time-lapse images were captured at a total of 100 frames. Recordings were started 6 min after the coverslip was placed in the chamber. The stacks of representative images were imported into NIH ImageJ software and converted to QuickTime movies. A mitochondrion was considered stopped if it remained stationary for the entire recording period; a motile one was counted only if it displaced at least 5 μm. To trace axonal anterograde or retrograde movement of mitochondria and to count stationary ones, kymographs were made as described previously (30,64) with extra plug-ins for ImageJ (NIH). Briefly, we used the 'Straighten' plugin to straighten curved axons, and the 'Grouped ZProjector' to z-axially project re-sliced time-lapse images. The height of the kymographs represents recording time (500 s unless otherwise noted), while the width represents the length (μm) of the axon imaged. Counts were averaged from 100 frames for each time-lapse image to ensure accuracy of stationary and motile events. Relative mitochondrial motility is described as the percentage of anterograde, retrograde or stationary events of total mitochondria. Measurements are presented as mean ± SEM. Statistical analyses were performed using unpaired Student's *t*-tests.

Preparation of mitochondria-enriched fractions

Mitochondria-enriched fraction was prepared from the forebrains of WT or mutant hAPP Tg (CaMKIIa-tTA x tet-APPswe/ind) mice at the age of 10–13 months (31), or from the cortices of AD patients or control subjects by Percoll gradient centrifugation as described previously (32,33). In brief, brain tissues were homogenized in ice-cold mitochondrial isolation buffer (IB, 0.32 M sucrose, 1 mM EDTA, 5 mM HEPES, pH 7.4). Homogenates were centrifuged at 1300*g* for 3 min, the supernatant was collected, and the pellet

was resuspended with IB and recentrifuged at 1300*g* for 3 min. The combined first and second supernatant was centrifuged at 21 000*g* for 10 min and the pellet was resuspended in 12 ml 15% Percoll. Two milliliters of the 15% Percoll suspension was overlaid on freshly prepared Percoll gradient containing 3.5 ml of 23% Percoll layered above 3.5 ml of 40% Percoll. The gradient was separated by centrifugation at 30 000*g* for 5 min. The mitochondrial fraction was harvested from the interface of the 23 and 40% Percoll layers, supplemented with 0.5 ml of 10 mg/ml BSA in 3 ml IB, centrifuged at 16 000*g* for 10 min, and then resuspended in IB. Protein concentrations of mitochondria-enriched membrane fraction were determined by BCA protein assay (Pierce Chemical Co.) using BSA standards. Equal amounts of proteins were processed for SDS–PAGE and immunoblotting on the same membranes after stripping between each application of the antibody.

Immunoisolation of Parkin-associated mitochondria

Brain tissues from WT or mutant hAPP Tg mice were homogenized in the buffer [10 mM HEPES (pH 7.4), 1 mM EDTA, 0.25 M sucrose and protease inhibitors] and centrifuged at 800*g* for 10 min, and then the supernatant was collected. The pellet was re-suspended in the homogenization buffer using a glass rod with 3–4 gentle strokes of the 30-ml Dounce Homogenizer pestle and re-centrifuged at 800*g* for 10 min. The combined first and second supernatants were centrifuged at 3500*g* for 10 min and then collected for high-speed centrifugation at 20 000*g* for 10 min. The pellet was re-suspended in the homogenization buffer using a glass rod with 3–4 gentle strokes of the 30-ml Dounce Homogenizer and re-centrifuged at 20 000*g* for 10 min. The pellet was then re-suspended in the homogenization buffer and subjected to immunoisolation with tosylated linker-coated superparamagnetic beads (Dynabeads M-450 Subcellular; Invitrogen) as previously described (44,45,65). For all subsequent steps, beads were collected with a magnetic device (MPC; Invitrogen). After washing once for 5 min in PBS (pH 7.4) with 0.1% BSA at 4°C, the linker-coated beads (1.4 mg) were incubated with 1 μg anti-Parkin mAb, or control mouse IgG overnight at 4°C on a rotator. After incubation, the beads were washed four times (5 min each) in PBS [pH 7.4] with 0.1% BSA at 4°C, and then re-suspended in an incubation buffer containing PBS [pH 7.4], 2 mM EDTA, 5% fetal bovine serum. Approximately 300 μg of light membrane fraction from WT or mutant hAPP Tg mouse brains were mixed with incubation buffer containing beads (final reaction volume 1 ml) and incubated for 4 h at 4°C on a rotator. After incubation, the beads were collected with a magnetic device and washed five times with the incubation buffer and three times with PBS for 10 min each and then resolved by 4–12% Bis–Tris PAGE for sequential western blots on the same membranes after stripping between each application of the antibody. For semi-quantitative analysis, protein bands detected by ECL were scanned into Adobe Photoshop CS6, and analyzed using NIH ImageJ.

Preparation of oligomeric Aβ

Oligomeric Aβ1–42 was prepared as previously described (20,48,49). Aβ1–42 peptide (Sigma) was diluted in 1,1,1,3,3,3-hexafluoro-2-propanol to 1 mM using a glass gas-tight Hamilton syringe with a Teflon plunger. The clear solution was then aliquoted in microcentrifuge tubes, followed by evaporation in the fume hood over night at room temperature, and it was then dried under vacuum for 1 h in a speedVac (DyNA Vap, Labnet). Peptide film was diluted in DMSO to 5 mM and sonicated for 10 min in bath sonicator. The peptide solution was resuspended in cold Neurobasal medium with B27 to 100 μM and immediately vortexed for 30 s; the solution was then incubated at 4°C for 24 h before applying to cultured cortical neurons.

Transmission electron microscopy

Hippocampi from AD patient brains and control subjects were cut into small specimens (one dimension < 1 mm) and fixed in Trumps fixative (Electron Microscopy Sciences) for 2 h at room temperature. The sections were then washed by 0.1 M Cacodylate buffer, and postfixed in 1% osmium tetroxide, followed by dehydrating in ethanol and embedding using the EM bed 812 kit (Electron Microscopy Sciences) according to a stand procedure. Images were taken on a JEOL 100 C× transmission electron microscope (Division of Life Sciences, Rutgers University Electron Imaging Facility). For quantitative studies, the number of mitochondria within autophagic vacuole (AV)-like organelles in neuronal perikarya and the number of total and abnormal mitochondria were counted from electron micrographs. Abnormal mitochondria were defined as having swollen round shape, and reduced, disorganized or loss of internal cristae (18). AVs were characterized by double-membrane structures surrounding mitochondria (AVi) or other organelles or vesicles, or containing partially degraded cytoplasmic material with higher electron density (AVd) (44,54,66). Glial cells were excluded on the basis of their nuclear morphology and chromatin patterns. Quantification analysis was performed blindly to condition.

Semi-quantitative RT-PCR analysis

Total RNA was isolated from human brain tissues using Trizol reagent (Invitrogen) according to the manufacturer's instructions. AMV reverse transcriptase XL (Takara) was used to synthesize the first-strand of cDNA from an equal amount of the RNA sample (0.5 μg). The newly synthesized cDNA templates were further amplified by *Takara Ex Taq* HS polymerase (Takara). Twenty-five to thirty-five cycles of PCR were used to cover the linear range of the PCR amplification. The human PARK2 gene-specific primers 5′-TTGACCCAGGGTCCATCTTGC-3′ and 5′- TGCTGGTACCGGTTG TACTGC-3′ were used to amplify a 452-bp fragment of the PARK2 gene coding region. The primers 5′-TTCCTTCCTGGGCATGGA GTC-3′ and 5′- ATTTGCGGTGGACGATGGAGG-3′ were used to amplify a 329-bp fragment of the human β-actin gene for internal controls. The samples were further analyzed on a 1.5% agarose gel. NIH ImageJ software was used to analyze the data.

Supplementary Material

Supplementary Material is available at *HMG* online.

Acknowledgements

We thank Z.-H. Sheng for important reagents; Y. Xie for technical help; E. Gavin, D. Ling, J. Filtes, R. Pillai, A. Yao, D. Aikal and other members in Q.C lab for their research assistance; Harvard Tissue Resource Center supported by National Institutes of Health grant HHSN-271-2013-00030C and Human Brain and Spinal Fluid Resource Center at UCLA for providing the postmortem brain specimens from AD patients and age-matched control subjects.

Conflict of Interest statement. None declared.

Funding

This research was supported by the National Institutes of Health (R00AG033658 and R01NS089737 to Q.C.); and the Charles & Johanna Busch Biomedical Award (to Q.C.).

References

1. Fukui, H. and Moraes, C.T. (2008) The mitochondrial impairment, oxidative stress and neurodegeneration connection: reality or just an attractive hypothesis? *Trends Neurosci.*, **31**, 251–256.
2. Swerdlow, R.H., Burns, J.M. and Khan, S.M. (2010) The Alzheimer's disease mitochondrial cascade hypothesis. *J. Alzheimers Dis.*, **20**(Suppl. 2), S265–S279.
3. Gibson, G.E. and Shi, Q. (2010) A mitocentric view of Alzheimer's disease suggests multi-faceted treatments. *J. Alzheimers Dis.*, **20**(Suppl. 2), S591–S607.
4. Gauthier, S., Reisberg, B., Zaudig, M., Petersen, R.C., Ritchie, K., Broich, K., Belleville, S., Brodaty, H., Bennett, D., Chertkow, H. *et al.* (2006) Mild cognitive impairment. *Lancet*, **367**, 1262–1270.
5. Mosconi, L. (2005) Brain glucose metabolism in the early and specific diagnosis of Alzheimer's disease. FDG-PET studies in MCI and AD. *Eur. J. Nucl. Med. Mol. Imaging*, **32**, 486–510.
6. Baloyannis, S.J. (2006) Mitochondrial alterations in Alzheimer's disease. *J. Alzheimers Dis.*, **9**, 119–126.
7. Hirai, K., Aliev, G., Nunomura, A., Fujioka, H., Russell, R.L., Atwood, C.S., Johnson, A.B., Kress, Y., Vinters, H.V., Tabaton, M. *et al.* (2001) Mitochondrial abnormalities in Alzheimer's disease. *J. Neurosci.*, **21**, 3017–3023.
8. Moreira, P.I., Siedlak, S.L., Wang, X., Santos, M.S., Oliveira, C.R., Tabaton, M., Nunomura, A., Szweda, L.I., Aliev, G., Smith, M.A. *et al.* (2007) Autophagocytosis of mitochondria is prominent in Alzheimer disease. *J. Neuropathol. Exp. Neurol.*, **66**, 525–532.
9. Court, F.A. and Coleman, M.P. (2012) Mitochondria as a central sensor for axonal degenerative stimuli. *Trends Neurosci.*, **35**, 364–372.
10. Du, H., Guo, L. and Yan, S.S. (2012) Synaptic mitochondrial pathology in Alzheimer's disease. *Antioxid. Redox. Signal*, **16**, 1467–1475.
11. Reddy, P.H. (2013) Amyloid beta-induced glycogen synthase kinase 3beta phosphorylated VDAC1 in Alzheimer's disease: implications for synaptic dysfunction and neuronal damage. *Biochim. Biophys. Acta.*, **1832**, 1913–1921.
12. Chu, C.T. (2010) A pivotal role for PINK1 and autophagy in mitochondrial quality control: implications for Parkinson disease. *Hum. Mol. Genet.*, **19**, R28–R37.
13. Mishra, P. and Chan, D.C. (2014) Mitochondrial dynamics and inheritance during cell division, development and disease. *Nat. Rev. Mol. Cell Biol.*, **15**, 634–646.
14. Sheng, Z.H. (2014) Mitochondrial trafficking and anchoring in neurons: New insight and implications. *J. Cell Biol.*, **204**, 1087–1098.
15. Sheng, Z.H. and Cai, Q. (2012) Mitochondrial transport in neurons: impact on synaptic homeostasis and neurodegeneration. *Nat. Rev. Neurosci.*, **13**, 77–93.
16. Youle, R.J. and Narendra, D.P. (2011) Mechanisms of mitophagy. *Nat. Rev. Mol. Cell Biol.*, **12**, 9–14.
17. Calkins, M.J., Manczak, M., Mao, P., Shirendeb, U. and Reddy, P.H. (2011) Impaired mitochondrial biogenesis, defective axonal transport of mitochondria, abnormal mitochondrial dynamics and synaptic degeneration in a mouse model of Alzheimer's disease. *Hum. Mol. Genet.*, **20**, 4515–4529.
18. Trushina, E., Nemutlu, E., Zhang, S., Christensen, T., Camp, J., Mesa, J., Siddiqui, A., Tamura, Y., Sesaki, H., Wengenack, T.M. *et al.* (2012) Defects in mitochondrial dynamics and metabolomic signatures of evolving energetic stress in mouse models of familial Alzheimer's disease. *PLoS One*, **7**, e32737.
19. Devi, L., Prabhu, B.M., Galati, D.F., Avadhani, N.G. and Anandatheerthavarada, H.K. (2006) Accumulation of amyloid precursor protein in the mitochondrial import channels of human Alzheimer's disease brain is associated with mitochondrial dysfunction. *J. Neurosci.*, **26**, 9057–9068.
20. Du, H., Guo, L., Yan, S., Sosunov, A.A., McKhann, G.M. and Yan, S.S. (2010) Early deficits in synaptic mitochondria in an Alzheimer's disease mouse model. *Proc. Natl Acad. Sci. USA*, **107**, 18670–18675.
21. Manczak, M., Calkins, M.J. and Reddy, P.H. (2011) Impaired mitochondrial dynamics and abnormal interaction of amyloid beta with mitochondrial protein Drp1 in neurons from patients with Alzheimer's disease: implications for neuronal damage. *Hum. Mol. Genet.*, **20**, 2495–2509.
22. Wang, X., Su, B., Siedlak, S.L., Moreira, P.I., Fujioka, H., Wang, Y., Casadesus, G. and Zhu, X. (2008) Amyloid-beta overproduction causes abnormal mitochondrial dynamics via differential modulation of mitochondrial fission/fusion proteins. *Proc. Natl Acad. Sci. USA*, **105**, 19318–19323.
23. Abramov, A.Y., Canevari, L. and Duchen, M.R. (2004) Beta-amyloid peptides induce mitochondrial dysfunction and oxidative stress in astrocytes and death of neurons through activation of NADPH oxidase. *J. Neurosci.*, **24**, 565–575.
24. Keller, J.N., Pang, Z., Geddes, J.W., Begley, J.G., Germeyer, A., Waeg, G. and Mattson, M.P. (1997) Impairment of glucose and glutamate transport and induction of mitochondrial oxidative stress and dysfunction in synaptosomes by amyloid beta-peptide: role of the lipid peroxidation product 4-hydroxynonenal. *J. Neurochem.*, **69**, 273–284.
25. Manczak, M., Anekonda, T.S., Henson, E., Park, B.S., Quinn, J. and Reddy, P.H. (2006) Mitochondria are a direct site of A beta accumulation in Alzheimer's disease neurons: implications for free radical generation and oxidative damage in disease progression. *Hum. Mol. Genet.*, **15**, 1437–1449.
26. Du, H., Guo, L., Fang, F., Chen, D., Sosunov, A.A., McKhann, G.M., Yan, Y., Wang, C., Zhang, H., Molkentin, J.D. *et al.* (2008) Cyclophilin D deficiency attenuates mitochondrial and neuronal perturbation and ameliorates learning and memory in Alzheimer's disease. *Nat. Med.*, **14**, 1097–1105.
27. Lustbader, J.W., Cirilli, M., Lin, C., Xu, H.W., Takuma, K., Wang, N., Caspersen, C., Chen, X., Pollak, S., Chaney, M. *et al.* (2004) ABAD directly links Abeta to mitochondrial toxicity in Alzheimer's disease. *Science*, **304**, 448–452.
28. Mattson, M.P., Partin, J. and Begley, J.G. (1998) Amyloid beta-peptide induces apoptosis-related events in synapses and dendrites. *Brain Res.*, **807**, 167–176.
29. Mucke, L., Masliah, E., Yu, G.Q., Mallory, M., Rockenstein, E.M., Tatsuno, G., Hu, K., Kholodenko, D., Johnson-Wood, K. and McConlogue, L. (2000) High-level neuronal expression of abeta 1–42 in wild-type human amyloid protein precursor transgenic mice: synaptotoxicity without plaque formation. *J. Neurosci.*, **20**, 4050–4058.
30. Cai, Q., Zakaria, H.M., Simone, A. and Sheng, Z.H. (2012) Spatial parkin translocation and degradation of damaged mitochondria via mitophagy in live cortical neurons. *Curr. Biol.*, **22**, 545–552.
31. Jankowsky, J.L., Slunt, H.H., Gonzales, V., Savonenko, A.V., Wen, J.C., Jenkins, N.A., Copeland, N.G., Younkin, L.H., Lester, H.A., Younkin, S.G. *et al.* (2005) Persistent amyloidosis

following suppression of Abeta production in a transgenic model of Alzheimer disease. *PLoS Med.*, **2**, e355.
32. Cai, Q., Gerwin, C. and Sheng, Z.H. (2005) Syntabulin-mediated anterograde transport of mitochondria along neuronal processes. *J. Cell Biol.*, **170**, 959–969.
33. Sims, N.R. (1990) Rapid isolation of metabolically active mitochondria from rat brain and subregions using Percoll density gradient centrifugation. *J. Neurochem.*, **55**, 698–707.
34. Chan, N.C., Salazar, A.M., Pham, A.H., Sweredoski, M.J., Kolawa, N.J., Graham, R.L., Hess, S. and Chan, D.C. (2011) Broad activation of the ubiquitin-proteasome system by Parkin is critical for mitophagy. *Hum. Mol. Genet.*, **20**, 1726–1737.
35. Yoshii, S.R., Kishi, C., Ishihara, N. and Mizushima, N. (2011) Parkin mediates proteasome-dependent protein degradation and rupture of the outer mitochondrial membrane. *J. Biol. Chem.*, **286**, 19630–19640.
36. Chu, C.T., Ji, J., Dagda, R.K., Jiang, J.F., Tyurina, Y.Y., Kapralov, A.A., Tyurin, V.A., Yanamala, N., Shrivastava, I.H., Mohammadyani, D. *et al.* (2013) Cardiolipin externalization to the outer mitochondrial membrane acts as an elimination signal for mitophagy in neuronal cells. *Nat. Cell Biol.*, **15**, 1197–1205.
37. Hansson Petersen, C.A., Alikhani, N., Behbahani, H., Wiehager, B., Pavlov, P.F., Alafuzoff, I., Leinonen, V., Ito, A., Winblad, B., Glaser, E. *et al.* (2008) The amyloid beta-peptide is imported into mitochondria via the TOM import machinery and localized to mitochondrial cristae. *Proc. Natl Acad. Sci. USA*, **105**, 13145–13150.
38. Hedskog, L., Pinho, C.M., Filadi, R., Ronnback, A., Hertwig, L., Wiehager, B., Larssen, P., Gellhaar, S., Sandebring, A., Westerlund, M. *et al.* (2013) Modulation of the endoplasmic reticulum-mitochondria interface in Alzheimer's disease and related models. *Proc. Natl Acad. Sci. USA*, **110**, 7916–7921.
39. Xie, H., Guan, J., Borrelli, L.A., Xu, J., Serrano-Pozo, A. and Bacskai, B.J. (2013) Mitochondrial alterations near amyloid plaques in an Alzheimer's disease mouse model. *J. Neurosci.*, **33**, 17042–17051.
40. Bingol, B., Tea, J.S., Phu, L., Reichelt, M., Bakalarski, C.E., Song, Q., Foreman, O., Kirkpatrick, D.S. and Sheng, M. (2014) The mitochondrial deubiquitinase USP30 opposes parkin-mediated mitophagy. *Nature*, **510**, 370–375.
41. Birsa, N., Norkett, R., Wauer, T., Mevissen, T.E., Wu, H.C., Foltynie, T., Bhatia, K., Hirst, W.D., Komander, D., Plun-Favreau, H. *et al.* (2014) Lysine 27 ubiquitination of the mitochondrial transport protein miro is dependent on serine 65 of the parkin ubiquitin ligase. *J. Biol. Chem.*, **289**, 14569–14582.
42. Liu, S., Sawada, T., Lee, S., Yu, W., Silverio, G., Alapatt, P., Millan, I., Shen, A., Saxton, W., Kanao, T. *et al.* (2012) Parkinson's disease-associated kinase PINK1 regulates Miro protein level and axonal transport of mitochondria. *PLoS Genet.*, **8**, e1002537.
43. Wang, X., Winter, D., Ashrafi, G., Schlehe, J., Wong, Y.L., Selkoe, D., Rice, S., Steen, J., LaVoie, M.J. and Schwarz, T.L. (2011) PINK1 and Parkin target Miro for phosphorylation and degradation to arrest mitochondrial motility. *Cell*, **147**, 893–906.
44. Cai, Q., Lu, L., Tian, J.H., Zhu, Y.B., Qiao, H. and Sheng, Z.H. (2010) Snapin-regulated late endosomal transport is critical for efficient autophagy-lysosomal function in neurons. *Neuron*, **68**, 73–86.
45. Ye, X. and Cai, Q. (2014) Snapin-mediated BACE1 retrograde transport is essential for its degradation in lysosomes and regulation of APP processing in neurons. *Cell Rep.*, **6**, 24–31.
46. Lee, S., Sato, Y. and Nixon, R.A. (2011) Lysosomal proteolysis inhibition selectively disrupts axonal transport of degradative organelles and causes an Alzheimer's-like axonal dystrophy. *J. Neurosci.*, **31**, 7817–7830.
47. Shukkur, E.A., Shimohata, A., Akagi, T., Yu, W., Yamaguchi, M., Murayama, M., Chui, D., Takeuchi, T., Amano, K., Subramhanya, K.H. *et al.* (2006) Mitochondrial dysfunction and tau hyperphosphorylation in Ts1Cje, a mouse model for Down syndrome. *Hum. Mol. Genet.*, **15**, 2752–2762.
48. Rui, Y., Tiwari, P., Xie, Z. and Zheng, J.Q. (2006) Acute impairment of mitochondrial trafficking by beta-amyloid peptides in hippocampal neurons. *J. Neurosci.*, **26**, 10480–10487.
49. Vossel, K.A., Zhang, K., Brodbeck, J., Daub, A.C., Sharma, P., Finkbeiner, S., Cui, B. and Mucke, L. (2010) Tau reduction prevents Abeta-induced defects in axonal transport. *Science*, **330**, 198.
50. Ashrafi, G., Schlehe, J.S., LaVoie, M.J. and Schwarz, T.L. (2014) Mitophagy of damaged mitochondria occurs locally in distal neuronal axons and requires PINK1 and Parkin. *J. Cell Biol.*, **206**, 655–670.
51. Cai, Q., Zakaria, H.M. and Sheng, Z.H. (2012) Long time-lapse imaging reveals unique features of PARK2/Parkin-mediated mitophagy in mature cortical neurons. *Autophagy*, **8**, 976–978.
52. Moreira, P.I., Siedlak, S.L., Wang, X., Santos, M.S., Oliveira, C.R., Tabaton, M., Nunomura, A., Szweda, L.I., Aliev, G., Smith, M.A. *et al.* (2007) Increased autophagic degradation of mitochondria in Alzheimer disease. *Autophagy*, **3**, 614–615.
53. Maday, S., Wallace, K.E. and Holzbaur, E.L. (2012) Autophagosomes initiate distally and mature during transport toward the cell soma in primary neurons. *J. Cell Biol.*, **196**, 407–417.
54. Nixon, R.A., Wegiel, J., Kumar, A., Yu, W.H., Peterhoff, C., Cataldo, A. and Cuervo, A.M. (2005) Extensive involvement of autophagy in Alzheimer disease: an immuno-electron microscopy study. *J. Neuropathol. Exp. Neurol.*, **64**, 113–122.
55. Yu, W.H., Cuervo, A.M., Kumar, A., Peterhoff, C.M., Schmidt, S.D., Lee, J.H., Mohan, P.S., Mercken, M., Farmery, M.R., Tjernberg, L.O. *et al.* (2005) Macroautophagy–a novel Beta-amyloid peptide-generating pathway activated in Alzheimer's disease. *J. Cell Biol.*, **171**, 87–98.
56. Boland, B., Kumar, A., Lee, S., Platt, F.M., Wegiel, J., Yu, W.H. and Nixon, R.A. (2008) Autophagy induction and autophagosome clearance in neurons: relationship to autophagic pathology in Alzheimer's disease. *J. Neurosci.*, **28**, 6926–6937.
57. Lee, J.H., Yu, W.H., Kumar, A., Lee, S., Mohan, P.S., Peterhoff, C.M., Wolfe, D.M., Martinez-Vicente, M., Massey, A.C., Sovak, G. *et al.* (2010) Lysosomal proteolysis and autophagy require presenilin 1 and are disrupted by Alzheimer-related PS1 mutations. *Cell*, **141**, 1146–1158.
58. Yang, D.S., Stavrides, P., Mohan, P.S., Kaushik, S., Kumar, A., Ohno, M., Schmidt, S.D., Wesson, D., Bandyopadhyay, U., Jiang, Y. *et al.* (2011) Reversal of autophagy dysfunction in the TgCRND8 mouse model of Alzheimer's disease ameliorates amyloid pathologies and memory deficits. *Brain*, **134**, 258–277.
59. Gregori, L., Fuchs, C., Figueiredo-Pereira, M.E., Van Nostrand, W.E. and Goldgaber, D. (1995) Amyloid beta-protein inhibits ubiquitin-dependent protein degradation in vitro. *J. Biol. Chem.*, **270**, 19702–19708.
60. Tseng, B.P., Green, K.N., Chan, J.L., Blurton-Jones, M. and LaFerla, F.M. (2008) Abeta inhibits the proteasome and enhances amyloid and tau accumulation. *Neurobiol. Aging*, **29**, 1607–1618.

61. Keller, J.N., Hanni, K.B. and Markesbery, W.R. (2000) Impaired proteasome function in Alzheimer's disease. *J. Neurochem.*, **75**, 436–439.
62. Braak, H. and Braak, E. (1991) Demonstration of amyloid deposits and neurofibrillary changes in whole brain sections. *Brain Pathol.*, **1**, 213–216.
63. Banker, G.A. and Cowan, W.M. (1979) Further observations on hippocampal neurons in dispersed cell culture. *J. Comp. Neurol.*, **187**, 469–493.
64. Kang, J.S., Tian, J.H., Pan, P.Y., Zald, P., Li, C., Deng, C. and Sheng, Z.H. (2008) Docking of axonal mitochondria by syntaphilin controls their mobility and affects short-term facilitation. *Cell*, **132**, 137–148.
65. Zhou, B., Cai, Q., Xie, Y. and Sheng, Z.H. (2012) Snapin recruits dynein to BDNF-TrkB signaling endosomes for retrograde axonal transport and is essential for dendrite growth of cortical neurons. *Cell Rep.*, **2**, 42–51.
66. Klionsky, D.J., Abdalla, F.C., Abeliovich, H., Abraham, R.T., Acevedo-Arozena, A., Adeli, K., Agholme, L., Agnello, M., Agostinis, P., Aguirre-Ghiso, J.A. *et al.* (2012) Guidelines for the use and interpretation of assays for monitoring autophagy. *Autophagy*, **8**, 445–544.